Microscale Thermophysical Engineering, 7:000–000, 2003

ISSN: 1089-3954 print/1091-7640 online
DOI: 10.1080/10893950390243581

Taylor & Francis
Taylor & Francis Group

A UNIFIED ENGINEERING MODEL FOR STEADY AND QUASI-STEADY SHEAR-DRIVEN GAS MICROFLOWS

P. Bahukudumbi, Jae Hyun Park, and Ali Beskok
Mechanical Engineering Department, Texas A&M University, College Station, Texas 77843, USA

We analyze one-dimensional plane Couette flows in the entire Knudsen regime with the objective of modeling shear-driven rarefied gas flows encountered in various microelectromechanical system (MEMS) components. Using the linearized Boltzmann solutions available in the literature and hard sphere direct simulation Monte Carlo (DSMC) results, we develop a unified empirical model that includes analytical expressions for the velocity distribution and shear stress for steady plane Couette flows. We also present extension of this model to time-periodic oscillatory Couette flows. Comparisons between the extended model and ensemble averaged **unsteady** ***DSMC computations show good agreements in the quasi-steady flow limit, where the Stokes number (β) based on the plate separation distance and oscillation frequency is $\leq$ 0.25. Overall, the new model accurately predicts the velocity distribution and shear stress for steady and quasi-steady ($\beta \leq 0.25$) flows in a wide Knudsen number range ($Kn \leq 12$), and it is strictly valid for low subsonic flows with Mach number $\leq$ 0.3.***

Keywords rarefied Couette flow, oscillating Couette flow, velocity slip, direct simulation Monte Carlo

Shear-driven microflows are encountered in several MEMS applications, including micromotors, microaccelerometers, microbearings, and in computer hard-drives. The simplest approximation for these is the classical Couette flow, shown in Figure 1. Although the analytical solution of Couette flow seems trivial, a fundamental problem arises when the distance between the two plates (D) becomes comparable to the gas mean-free-path (λ). The ratio of these two length scales is known as the Knudsen number ($Kn = \lambda/\mathrm{D}$), where finite values of Kn shows onset of rarefaction effects. Based on the Knudsen number, gas flows are classified as continuum ($Kn < 0.01$), slip ($0.01 < Kn < 0.1$), transition ($0.1 < Kn < 10$), and free-molecular ($Kn > 10$) flow regimes [1]. A major portion of MEMS devices operate in the slip and early transitional flow regimes. Further miniaturization of device components will push this limit to the transition and free-molecular regimes. Successful design of such micro-fluidic systems requires development of generalized engineering models that are uniformly valid in a wide range of Knudsen regimes.

Figure 1

Manuscript received on December 6, 2002; accepted for publication on February 18, 2003.
Address correspondence to Ali Beskok, Mechanical Engineering Department, Texas A&M University, College Station, Texas 77843. E-mail: Abeskok@mengr.tamu.edu

NOMENCLATURE

D	distance separating two moving surfaces
Kn	Knudsen number: λ/D
Ma	Mach number
N_p	number of simulation molecules
P	pressure: ρRT
R	specific gas constant
T	temperature
U	lateral wall speed
U_0	oscillation amplitude
Y	nondimensional coordinate
c_0	most probable velocity; $\sqrt{2kT_o/m}$
d	molecular diameter
h	plate separation
k	modified Knudsen number: $(\sqrt{\pi}/2)Kn$
l_s	slip length
m	hard sphere molecule mass
n	number density
x	stream-wise direction
y	cross-flow direction

Greek symbols

α	slip coefficient
α_m	generalized slip coefficient
β	Stokes number: $\sqrt{\omega h^2/\nu}$
δ	inverse Knudsen number: $0.88845/Kn$
Δt	simulation time step
Δx	cell size
γ	Adiabatic index
λ	mean free path: $(\sqrt{2}\pi nd^2)^{-1}$
μ	dynamic viscosity: $(2RT_w/\pi)^{1/2}\rho_o\lambda$
μ_{eff}	effective dynamic viscosity
ν	kinematic viscosity
ω	angular velocity of oscillations
π_{xy}	shear stress, normalized with free molecular value
Π_{xy}	shear stress, normalized with continuum value
ρ	density
σ_v	tangential momentum accommodation coefficient
τ_{xy}	shear stress

Subscripts

c	Couette
cont	continuum
hs	hard sphere
o	reference
qs	quasi-steady
vhs	variable hard sphere
w	wall condition
∞	free-molecular

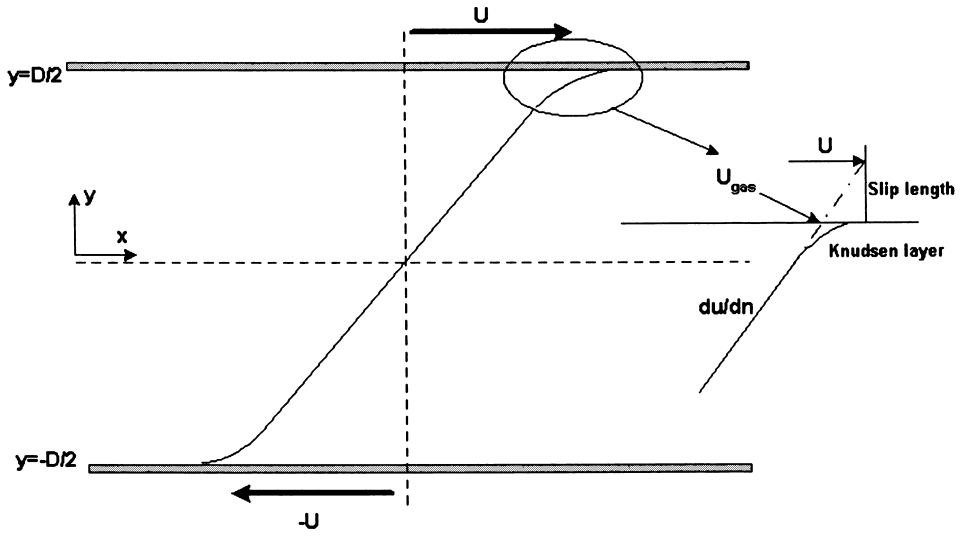

Figure 1. Schematic view of linear Couette flow and the corresponding velocity profile for rarefied gas flows. Inset shows the slip length concept l_s.

Simple nature of the plane Couette flow makes it the most studied boundary value problem in Kinetic Theory. Numerical analysis of rarefied gas flow in the entire Knudsen regime requires solution of the Boltzmann equation or atomistic simulation methods, such as the direct simulation Monte Carlo (DSMC) method of Bird [2]. In the following, we review some of the previous investigations of rarefied plane Couette flows. Gross and Ziering [3] applied moment methods to the linearized Boltzmann equation and analyzed plane Couette flows for hard sphere molecules. In separate studies, Willis [4] and Loyalka et al. [5] obtained accurate numerical solutions of the BGK Boltzmann equation for Couette flows, while Cercignani [6] and Saraf [7] provided analytical solutions using variational techniques. Sone et al. [8] investigated rarefied Couette flows using linearized Boltzmann equation for hard sphere molecules and obtained accurate results for the velocity profile, shear stress, and heat transfer in the entire flow regime. Nanbu [9] used a direct simulation method, which accurately models the collision integral term in the Boltzmann equation, and obtained exact solutions for steady Couette flows. Fan and Shen [10] developed an information preservation DSMC method and simulated low-speed rarefied Couette flows. Xue et al. [11] used Burnett equations to study micro-Couette flows in the slip and early transitional flow regimes. More recently, Veijola and Turowski [12] obtained an empirical expression for Couette flow shear stress that has a maximum absolute relative error of 0.7% in the entire Knudsen regime. They utilized this model to study the damping coefficient of laterally oscillating microstructures. A majority of these semi-analytical and numerical investigations are restricted to the study of macroscopic properties, such as shear drag; however, accurate velocity models for plane Couette flow are necessary for analyzing the dynamic response and viscous damping characteristics of laterally oscillating microstructures and slider heads utilized in magnetic disk storage units.

Beyond the slip flow regime, continuum-based formulations for rarefied gas flows require modified constitutive laws for stress tensor and heat flux vector, as well as new velocity slip and temperature jump boundary conditions [13]. For example, Burnett equations are derived from the Boltzmann equation via a second-order Chapman-Enskog expansion in Kn. Hence, the Burnett equations also require second-order slip conditions in Kn. Although such developments are important, simplified models using the Navier-Stokes equations with empirical corrections can find extended use in engineering applications. The current investigation is triggered by absence of simple analytical models for engineering analysis of shear-driven microflows that are valid in all Knudsen regimes. Hence, the current work has the following objectives:

1. Development of an empirical velocity model, which accurately predicts the velocity distribution in the bulk flow region for a wide range of Knudsen numbers ($Kn \leq 12$).
2. Development of an accurate shear stress model that is asymptotically consistent in the continuum and free molecular flow limits.

This paper is organized as follows: In the next section, we introduce a generalized slip coefficient and then develop an accurate analytical expression for the velocity distribution. Details of slip length comparisons are also included. In section 2, we present the shear stress model and investigate its asymptotic characteristics in the continuum and free molecular limits. In section 4 we present extension of the current model to

oscillatory Couette flows and validate it in the quasi-steady flow limit, using unsteady DSMC simulations. Finally, we present conclusions of our study.

1. VELOCITY MODEL

We consider rarefied gas flow between two infinite parallel plates, maintained at the same uniform temperature T_w and moving with a uniform velocity of $\pm U$, as shown in Figure 1. We investigate steady one-dimensional plane Couette flow induced between the plates subject to the following assumptions:

1. Gas molecules are hard spheres of uniform size and they undergo diffuse reflections with the surfaces ($\sigma_v = 1$).
2. Plate velocity is small compared to the mean thermal velocity ($U/\sqrt{2RT_w} \ll 1$).
3. Temperature fluctuations and viscous heating effects are negligible.

Velocity field in the slip flow region can be determined from the Navier-Stokes equations subject to the velocity-slip boundary condition. Neglecting the thermal creep effects, velocity slip condition is given by [14]

$$u - U = \frac{2 - \sigma_v}{\sigma_v} \alpha \lambda \frac{du}{dy}, \tag{1}$$

where u is the gas slip velocity, α is the slip coefficient, and σ_v is the tangential momentum accommodation coefficient ($\sigma_v = 1$ for diffuse reflections and $\sigma_v = 0$ for specular reflections). The value of the slip coefficient, originally derived by Maxwell, is $\alpha = 1$. More accurate values for the slip coefficient have been determined using Boltzmann equation, DSMC, and molecular dynamics simulations. For example, the theoretical model derived by Ohwada et al. [15] using linearized Boltzmann equation for hard sphere molecules predicts $\alpha = 1.111$ for $Kn \leq 0.1$.

Starting from the Navier-Stokes equations, and assuming steady fully developed *incompressible* flow, the streamwise momentum equation can be reduced to

$$\frac{d^2u}{dy^2} = 0. \tag{2}$$

The incompressible flow approximation is appropriate only for low Mach number flows, typically for $Ma < 0.3$, as we will demonstrate later in this section. Using the slip boundary condition given by equation (1), we obtain the following linear velocity distribution (u_c):

$$u_c(Y) = \frac{2U}{1 + 2\dfrac{2 - \sigma_v}{\sigma_v} \alpha Kn} \frac{y}{D}, \tag{3}$$

where $Kn = \lambda / D$. Utilizing this solution with $\alpha = 1.111$, Marques et al. [16] have shown that equation (3) is valid for $Kn \leq 0.25$.

Steady flow calculations by Sone et al. [8] using the linearized Boltzmann equation indicate that the bulk flow velocity profile is essentially linear for all Knudsen numbers;

however, a kinetic boundary layer (Knudsen layer) on the order of a mean free path starts to become dominant between the bulk flow and solid surfaces in the transition flow regime. The velocity distribution and other physical variables are subject to appreciable changes within the Knudsen layer, which can only be predicted by solution of the Boltzmann equation. Figure 1 shows a schematic drawing of the velocity profile, including the Knudsen layer effects. To validate Sone's linearized Boltzmann solutions, we performed a series of hard-sphere DSMC simulations at various Knudsen numbers and wall speeds. Our hard-sphere DSMC algorithm is based on an earlier algorithm presented by Garcia [17]. DSMC can be applied for modeling gas transport in the entire Knudsen regime. For the sake of brevity, we avoid description of the DSMC algorithm. The reader is referred to Bird [2], Muntz [18], Alexander and Garcia [19], and Oran et al. [20] for an introduction to the DSMC method, different molecular interaction models, and algorithmic details. In our simulations, solid surfaces were maintained at 273 K and they were assumed to be fully accommodating ($\sigma_v = 1$). We simulated argon gas with molecular mass $m = 6.63 \times 10^{-26} kg$ and hard sphere diameter $d_{hs} = 3.66 \times 10^{-10} m$. We note that collision diameter for hard-sphere molecules is independent of the relative velocity of the colliding molecules. This results in viscosity dependence on temperature in the form of $\mu_0 \propto T_o^{0.5}$. This trend is slightly different from a more reliable variable hard sphere (VHS) model, which has viscosity dependence on temperature in the form of $\mu_0 \propto T_o^{0.81}$ for argon molecules; however, it is noted that DSMC simulations for hard-sphere and variable hard-sphere molecules yield similar results when the flow is isothermal. Simulations were performed for a wide range of Knudsen and Mach numbers. A minimum of 20 cells across the channel width was used in the simulations, and the domain discretization always ensured a minimum of 3 cells per mean free path. With this discretization, we used $10,000$ hard-sphere particles and sampled our results for 1.0×10^6 time steps. The simulation time-step was $1/5^{th}$ of the mean collision time ($\lambda/\sqrt{2RT_o}$). These sets of parameters are sufficient to obtain accurate DSMC results [21].

In Figure 2 we present velocity profiles for linear Couette flow in the upper half of the channel at three different Knudsen numbers. The linearized Boltzmann solutions (triangles) and DSMC (circles) agree quite well, and they both predict essentially linear velocity distribution in the bulk flow region with significant slip effects for increased Kn. The Knudsen layers are also visible in the figure, and they become dominant especially in the transition flow regime, where $D \simeq \lambda$. The nondimensional results are valid for any monoatomic hard-sphere dilute gas. Figure 2 also shows the velocity distribution predicted using Maxwell's first-order slip model (dashed-lines). These analytical results are obtained using equation (3) with $\alpha = 1.111$, and the first-order slip solution is reasonable for $Kn \leq 0.1$.

Figure 2

Motivated by the linear velocity distribution in the bulk flow region, we introduce a correction to equation (1) (and similarly to equation (3)) using a modified slip coefficient α_m in the following form:

$$\alpha_m = \beta_0 + \beta_1 tan^{-1}(\beta_2 Kn^{\beta_3}), \tag{4}$$

where $\beta_i (i = 0, 1, 2, 3)$ are empirical constants that are obtained by comparing the slope of the velocity profile, obtained by the linearized Boltzmann solution of Sone et al. [8], with that obtained from equation (3) using α_m. Our objective in introducing this modified

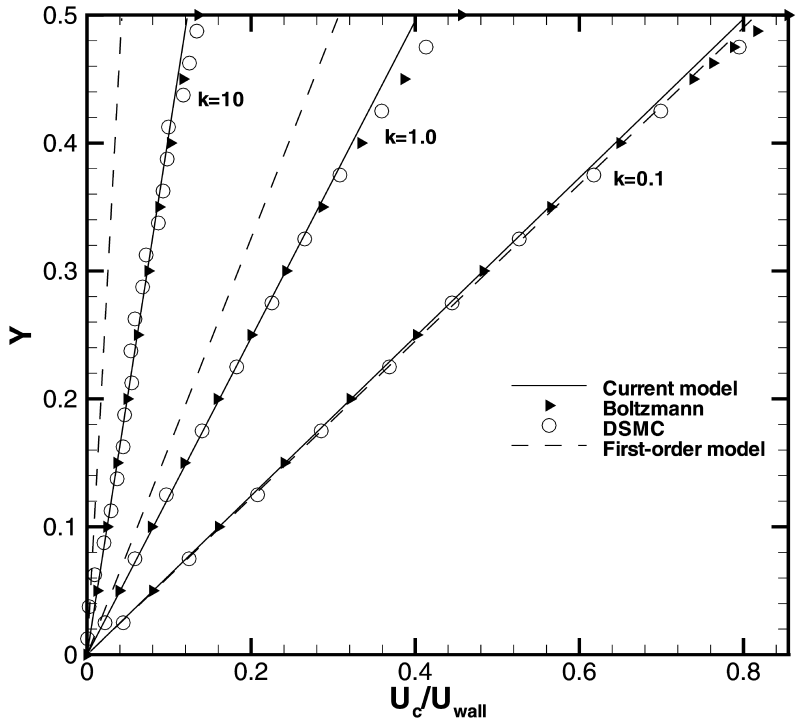

Figure 2. Velocity profiles for linear Couette flow in the upper-half of the channel at $k = 0.1$, 1.0, and 10.0. The wall speed corresponds to $Ma = 0.05$.

slip coefficient is to establish a velocity-slip boundary condition for the Navier-Stokes equation, which yields a solution that coincides with the linearized Boltzmann equation in the bulk flow region. The generalized velocity slip coefficient (α_m) is in essence a correction term applied to extend the validity of the original first-order slip boundary condition. We have determined $\beta_0 = 1.2977$, $\beta_1 = 0.71851$, $\beta_2 = -1.17488$, and $\beta_3 = 0.58642$ using a least square fit to the linearized Boltzmann solutions presented in [8].

In Figure 2 we also present the predictions obtained by the new model (solid lines). Unlike the first-order model, the unified model accurately matches the velocity profile in the bulk flow region for a wide range of Knudsen numbers. We tested our model against the DSMC solution up to $Kn = 12$. We note that the new model fails to predict the velocity distribution in the Knudsen layer. This is expected, as the model is based on the Navier-Stokes equations, and the velocity profiles cannot be different from a linear profile, as predicted by equation (2). For $Kn < 0.1$, presence of the Knudsen layer can be neglected by extrapolating the bulk flow toward the wall. When $Kn > 1$, the Knudsen layer occupies the entire channel. It is interesting to note that, for $Kn = 10$, we observe presence of a sublayer within the kinetic boundary layer, resulting in deviations from the linear velocity profile near the walls.

The results presented in Figure 2 are obtained for $Ma = 0.05$, and they exhibit rarefaction effects alone. Although the compressibility and viscous heating effects are

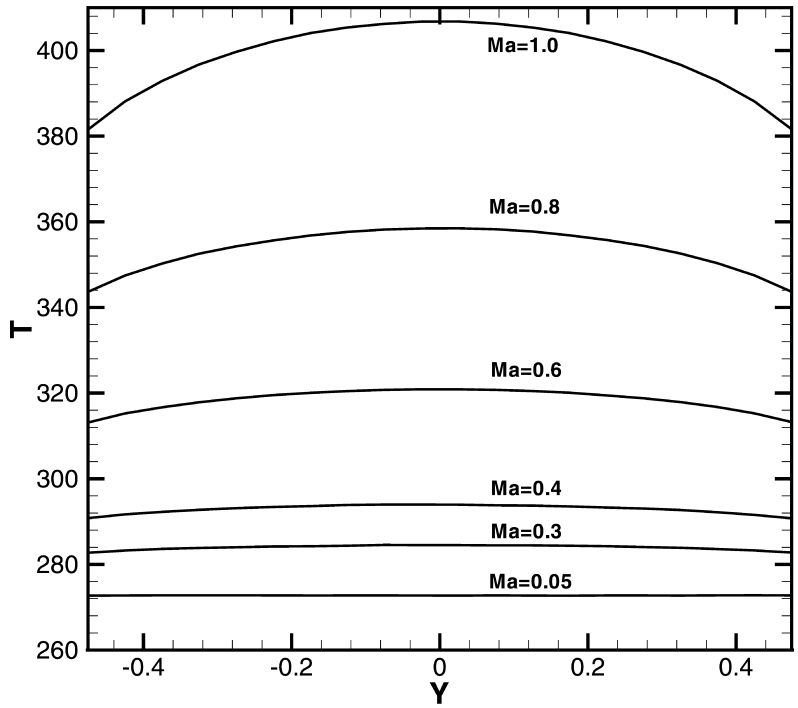

Figure 3. Temperature distribution across the channel, obtained by hard-sphere DSMC at $k = 1.0$ and at various wall speeds (Ma). Significant increase in the average temperature with increased Ma is due to viscous heating. Temperature jump effects are visible, as the walls are kept at 273 K.

insignificant for low speed flows, they become important for nonisothermal and high Mach number flows. Figure 3 shows temperature profiles obtained at $k = 1.0$ under varying wall velocities. The results are obtained by hard-sphere DSMC simulations, and they show significant increase in the mean temperature with increased Ma. Temperature jump effects are also visible in the figure, since the walls are kept at 273 K for all simulations. The reason for these temperature variations is viscous heating [13]. Increased compressibility effects for higher Mach number flows are in effect a manifestation of significant viscous heating.

Figure 4 shows the compressibility effects on Couette flow velocity distribution. The results are obtained using hard-sphere DSMC simulations at various wall speeds. The new velocity model and the linearized Boltzmann solution [8] exhibit significant deviations from the hard-sphere DSMC simulation results, when $Ma > 0.3$. These deviations are expected, as discussed in [22, 23]. To extend the velocity model for $Ma > 0.3$, a slip boundary condition that couples the velocity and temperature fields is necessary, as presented in [24]. For the range of simulations performed here, the maximum deviation of the new velocity model from the DSMC results is around 7% when $Ma = 0.5$, and the deviation is 14% when $Ma = 1.0$.

Velocity slip is usually characterized by a nondimensional parameter, known as the slip length (l_s), which is the distance from the solid wall, where the extrapolated bulk

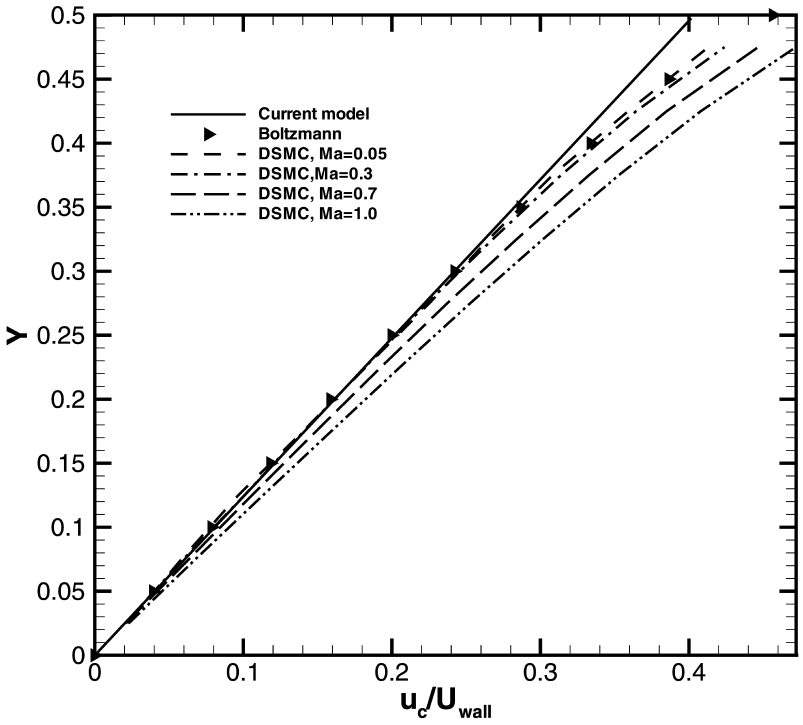

Figure 4. Couette flow velocity distribution in the upper-half of the channel at $k = 1.0$ at various wall speeds (Ma).

flow velocity is equal to the wall velocity (see Fig. 1). A no-slip boundary condition is equivalent to $l_s = 0$, whereas a slip boundary condition results in a finite slip length, $l_s > 0$. Bhattacharya and Lie [25] and Morris et al. [26] analyzed slip-length variation as a function of the Knudsen number using molecular dynamics and variable hard-sphere DSMC simulations. More recently, Wijesinghe and Hadjiconstantinou [27] presented slip length for Couette flows using hard-sphere DSMC simulations and compared it with the corresponding theoretical hard-sphere results. Following Bhattacharya and Lie [25], the velocity-slip boundary condition given by equation (1) can be written in terms of a nondimensional slip-length (l_s) as follows:

$$l_s = \frac{u\left(y = \dfrac{D}{2}\right) - U}{D\dfrac{\partial u(y)}{\partial y}} = \alpha Kn. \tag{5}$$

The velocity gradient $\partial u(y)/\partial y$ is determined from the velocity profile outside the Knudsen layer, as illustrated in Figure 1. Slip velocity at the surface ($u(y = D/2)$) is obtained by extrapolating the bulk-flow velocity profile to the wall. Figure 5 shows normalized slip length obtained from the hard-sphere DSMC simulations and the modified slip boundary condition expressed in terms of the normalized slip-length. These results are obtained

Figure 5

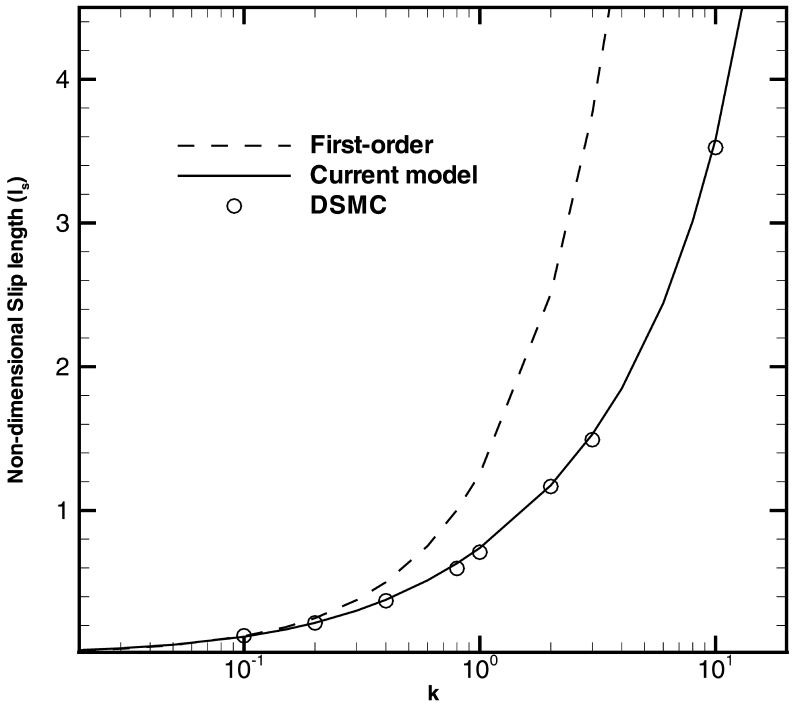

Figure 5. Normalized slip length (l_s) variation as a function of the modified Knudsen number k.

for $Ma = 0.05$. Slip length computed using the first-order slip model with $\alpha = 1.111$ deviates from the DSMC predictions for $k > 0.1$, as expected. The slip length computed using equation (5) with the generalized slip coefficient (α_m) is in good agreement with the DSMC results for a wide range of Knudsen numbers. Also, there are no discernible differences in the slip length results for $Ma \leq 0.3$.

2. SHEAR STRESS MODEL

Shear stress for Couette flows exhibits two distinct behaviors in the continuum and free molecular flow regimes. Using the classical constitutive laws utilized in the Navier-Stokes equations, shear stress for plane Couette flow is given by

$$\tau_{xy,cont} = \mu \frac{du}{dy} = -\mu \frac{2U}{D}, \tag{6}$$

where the viscosity $\mu = (2RT_w/\pi)^{1/2}\rho_o\lambda$ does not depend on pressure and the minus sign is due to direction of the shear stress on the fluid. Hydrodynamic approximation of shear stress is proportional to the velocity gradient (angular deformation rate for 1-D flow). This representation is also valid in the slip-flow regime with appropriate velocity slip corrections. In the free molecular flow regime, the shear stress is proportional to the

density and relative velocity of the plates, and it is given by [28]:

$$\tau_{xy,\infty} = -\rho_o U \sqrt{\frac{2RT_w}{\pi}}. \tag{7}$$

We note that this behavior is independent of the angular deformation rate ($\partial u/\partial y$). Hence, a free molecular shear stress exists even if $\partial u/\partial y \to 0$. This creates an inconsistency for a unified shear stress model that relates the angular deformation rate and shear stress using an effective viscosity model ($\mu_{eff} = (\partial u/\partial y)/\tau_{xy}$). It is evident that it is not possible to construct a shear stress model based on the Navier-Stokes–level constitutive equations that are uniformly valid in the entire Knudsen number regime. Veijola and Turowski [12] proposed a model for dynamic viscosity variation as a function of the Knudsen number. We note that their viscosity model is in essence a shear stress model with slip effects lumped into it. Hence, it cannot be used to predict the velocity distribution. The empirical model developed by Veijola and Turowski [12] is obtained by curve fitting to linearized Boltzmann solutions, and it is given by

$$\pi_{xy} = -\frac{2Kn}{1 + 2Kn + 0.2Kn^{0.788}\exp^{-0.1Kn}}, \tag{8}$$

where π_{xy} is the shear stress normalized with the free molecular shear stress. Cercignani [6] derived an analytical expression for shear stress using different molecular interaction models

$$\pi_{xy} = -\frac{a_1 Kn^2 + a_2 Kn^2}{a_1 Kn^2 + a_3 Kn + a_4}, \tag{9}$$

$$a_1 = 1.3056, \qquad a_2 = 2\pi, \qquad a_3 = 7.5939, \qquad a_4 = \pi.$$

The value of the coefficients a_1, a_2, a_3, and a_4 in equation (9) depends on the molecular interaction model used, and we present the coefficients corresponding to the hard-sphere molecules. Sone et al. [8] have obtained accurate numerical solutions for shear stress in the entire Knudsen regime. They also developed the following analytical solution valid for $Kn \to 0$, using perturbation expansions

$$\pi_{xy} = -\frac{\gamma_1 \pi Kn}{2(1 + 2\alpha Kn)}, \quad \gamma_1 = 1.270042, \qquad \alpha = 1.111.$$

In this paper, we present a shear stress model similar in form to the variational result of Cercignani [6] as shown below:

$$\pi_{xy} = -\frac{aKn^2 + 2bKn}{aKn^2 + cKn + b}, \tag{10}$$

$$a = 0.529690, \quad b = 0.602985, \quad c = 1.627666,$$

where the coefficients a, b, and c are obtained by a least-squares fit to the linearized Boltzmann solution of Sone et al. [8]. It is important to test the model for uniform

convergence to the correct continuum ($Kn \to 0$) and free-molecular ($Kn \to \infty$) limits. The shear stress model should result in consistent asymptotic expansions in both the continuum and free molecular limits, which may be important for further theoretical work that utilize perturbation expansions in Kn or Kn^{-1}. Taylor series expansions of the new model in the above-mentioned limits are given by

$$\frac{\tau_{xy}}{\tau_{xy,\infty}} = \pi_{xy} = 1 + \frac{2b-c}{a}\frac{1}{Kn} + \frac{-b-\left(\frac{2b-c}{a}\right)c}{a}\frac{1}{Kn^2} + O(Kn^{-3}) \quad \text{as } Kn \to \infty, \tag{11}$$

$$\frac{\tau_{xy}}{\tau_{xy,cont}} = \Pi_{xy} = 1 + \frac{a-2c}{2b}Kn + \frac{\left(\frac{2c-a}{b}\right)c - 2a}{2b}Kn^2 + O(Kn^3) \quad \text{as } Kn \to 0, \tag{12}$$

where the coefficients of the $O(Kn^i)$ terms ($i = \ldots, -2, -1, 1, 2, \ldots$) are corrections to the shear stress due to different orders of Kn dependence. It can be seen that the coefficient of the $O(Kn)$ term in the expansion for Π_{xy} is $\frac{a-2c}{2b} = -2.2601 \simeq -2\alpha = 2.222$. Comparing Eq. (12) with the asymptotic theory of Sone et al. (1990) in the continuum limit, we obtain that the two representations are similar up to the second-order terms in Kn.

In Figure 6 we compare the normalized shear stress π_{xy} predicted by the new model with our hard-sphere DSMC results, linearized Boltzmann solution of Sone et al. [8], and 4-moment solution of Gross and Ziering [3]. All solutions uniformly approach to the free-molecular flow shear stress limit, as $Kn \to \infty$; however, the asymptotic solution of Sone (derived for $Kn \to 0$) systematically deviates from the linearized Boltzmann and DSMC results for $Kn > 1.0$. Differences between the current hard-sphere DSMC results and the linearized Boltzmann solution are almost invisible in the figure. Any discrepancy in the numerical values can be attributed to the statistical nature of the DSMC. Table 1 compares the current shear stress model with other available analytical models. The new shear stress model has a maximum deviation of 0.3% from the linearized Boltzmann solution, whereas the disagreement is about 1% for variational solution of Cercignani et al. [6] and 0.7% for the empirical model of Veijola and Turowski [12]. Shear stress normalized by the corresponding continuum value is also plotted as a function of the modified Knudsen number in Figure 6. Good agreements between the new model and the linearized Boltzmann solutions are observed.

Figure 6

Table 1

The results presented in Figure 6 were obtained for $Ma = 0.05$ flow. We studied the shear stress variation as a function of the wall speed using hard-sphere DSMC simulations. Significant increases in the mean temperature with Ma were reported in Figure 3. Correspondingly, the maximum increase observed in the magnitude of the shear stress is about 6%, as the Mach number is increased from 0.05 to 1.0. Figure 7 shows normalized shear stress for $Ma = 0.05$ and $Ma = 1.0$ flows obtained at different Kn values. The new shear stress model is not as sensitive to the maximum wall speed as the velocity distribution.

Figure 7

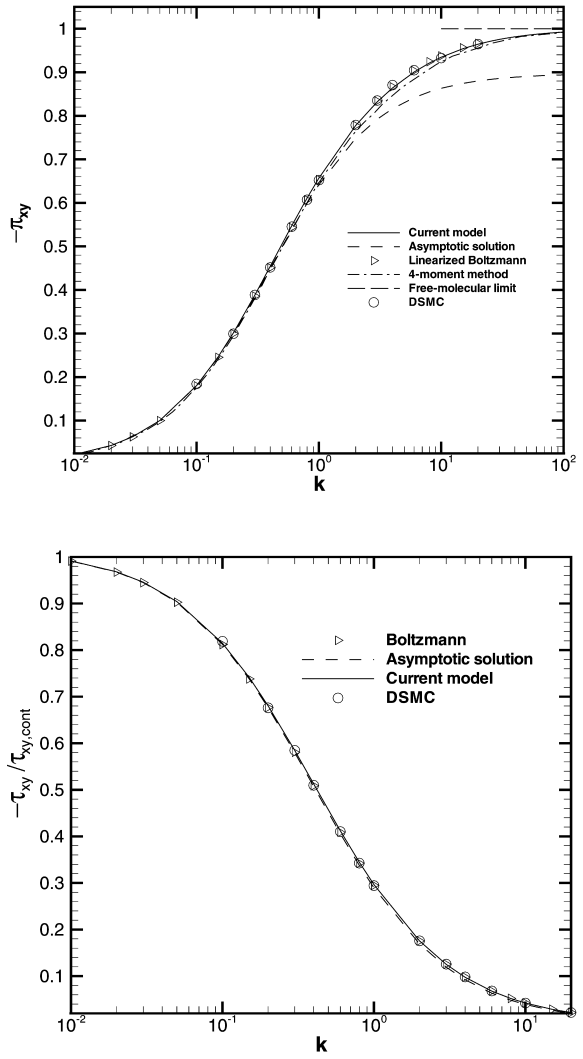

Figure 6. Variation of normalized shear stress with modified Knudsen number k. Top figure shows shear stress normalized with the free molecular value, whereas the bottom figure shows shear stress normalized with its corresponding Newtonian fluid continuum flow value.

3. OSCILLATORY COUETTE FLOWS

Oscillatory Couette flow, schematically shown in Figure 8, is the simplest approx- **Figure 8**
imation for time-periodic shear-driven gas flows encountered in several MEMS applica- **280**
tions, such as microaccelerometers, inertial sensors, and resonant filters. This flow is a variation of the Stokes' second problem with the inclusion of a wall bounding a thin fluid film of thickness h [29]. Although this classical problem has been investigated extensively using continuum-based flow models in the continuum and slip flow regimes [12], rarefaction effects in the transition and free molecular flow regimes have not been studied **285**

Table 1. Normalized wall shear stress (π_{xy}) variation as a function of the modified Knudsen number. Comparisons between the new model, linearized Boltzmann results, and several other analytical models are also included

k/π_{xy}	Sone et al. [8]	Current model	Cercignani [6]	Veijola & Turowski [12]
0.0001	0.0002	0.0002	0.0002	0.0002
0.005	0.0111	0.0111	0.0111	0.0111
0.01	0.0220	0.0220	0.0220	0.0219
0.05	0.1000	0.1001	0.1001	0.0996
0.1	0.1800	0.1800	0.1804	0.1789
0.15	0.2453	0.2454	0.2461	0.2441
0.2	0.2999	0.2999	0.3011	0.2985
0.3	0.3859	0.3861	0.3878	0.3848
0.4	0.4509	0.4512	0.4532	0.4503
0.6	0.5434	0.5438	0.5458	0.5435
0.8	0.6069	0.6072	0.6085	0.6071
1.0	0.6535	0.6536	0.6540	0.6535
1.5	0.7303	0.7299	0.7280	0.7294
2.0	0.7777	0.7771	0.7731	0.7760
3.0	0.8339	0.8333	0.8267	0.8314
4.0	0.8666	0.8663	0.8583	0.8643
6.0	0.9037	0.9037	0.8948	0.9027
8.0	0.9242	0.9246	0.9158	0.9252
10.0	0.9375	0.9380	0.9296	0.9401
15.0	0.9562	0.9570	0.9498	0.9619
20.0	0.9663	0.9670	0.9609	0.9732

in detail. In this section, we extend our steady flow velocity and shear stress models to include oscillatory Couette flows, and we validate our model using the *unsteady* DSMC simulations.

Velocity Model

Navier-Stokes equations, along with appropriate slip boundary conditions, can be used to describe the motion of a laterally oscillating plate floating over a thin viscous fluid film. We consider the rarefied gas flow between two infinite parallel plates that are a distance h apart, where the top plate oscillates harmonically in the lateral direction and the bottom plate is stationary. The following assumptions are made:

1. Lateral motion of the plate does not generate any streamwise pressure gradients.
2. Oscillation velocity is small compared to the mean thermal velocity of molecules.
3. Flow is isothermal and compressibility and viscous heating effects are negligible.

Under these simplifications, the momentum equation reduces to the following:

$$\frac{\partial u(y,t)}{\partial y} = \nu \frac{\partial^2 u(y,t)}{\partial y^2}, \tag{13}$$

where ν is the gas kinematic viscosity. An analytical solution of the above equation can be obtained for oscillatory flows with a specified frequency ω and amplitude U_0

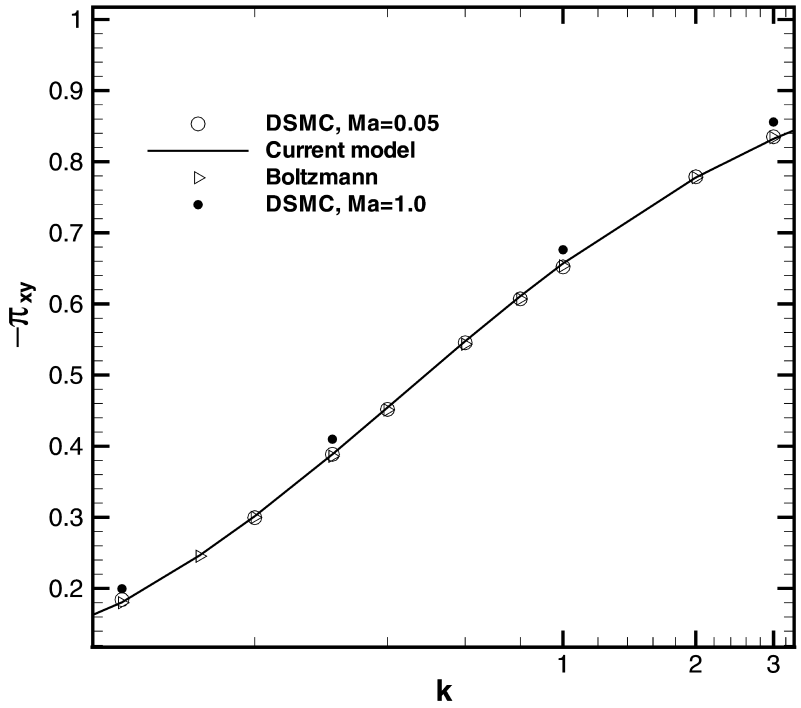

Figure 7. Normalized shear stress $-\pi_{xy}$ variation as a function of k at $Ma = 0.05$ and $Ma = 1.0$. DSMC results at $M = 1.0$ are included to examine the viscous heating effects on shear stress. Maximum increase in the shear stress is about 6% for $Ma \leq 1.0$ at any Kn.

as shown in [30]. For a sinusoidal velocity excitation, a velocity response of the form $u(y, t) = \Im\{V(y)\exp(j\omega t)\}$ is expected, where the symbol $\Im$ denotes the imaginary part of a complex expression. The amplitude $V(y)$ is governed by

$$j\omega V(y) = \nu \frac{\partial^2 V(y)}{\partial y^2} \tag{14}$$

or

$$\frac{\partial^2 V(y)}{\partial y^2} - \psi^2 V(y) = 0, \tag{15}$$

where $\psi = \sqrt{\frac{j\omega}{\nu}}$ is the complex frequency variable, and $j = \sqrt{-1}$. The generalized solution of the above equation can be written in the following form [12]:

$$V(y) = C_1 \sinh(\psi y) + C_2 \cosh(\psi y), \tag{16}$$

where the constants C_1 and C_2 are determined by applying the boundary conditions. The complex variable ψ can be expressed in terms of the Stokes number β, which represents

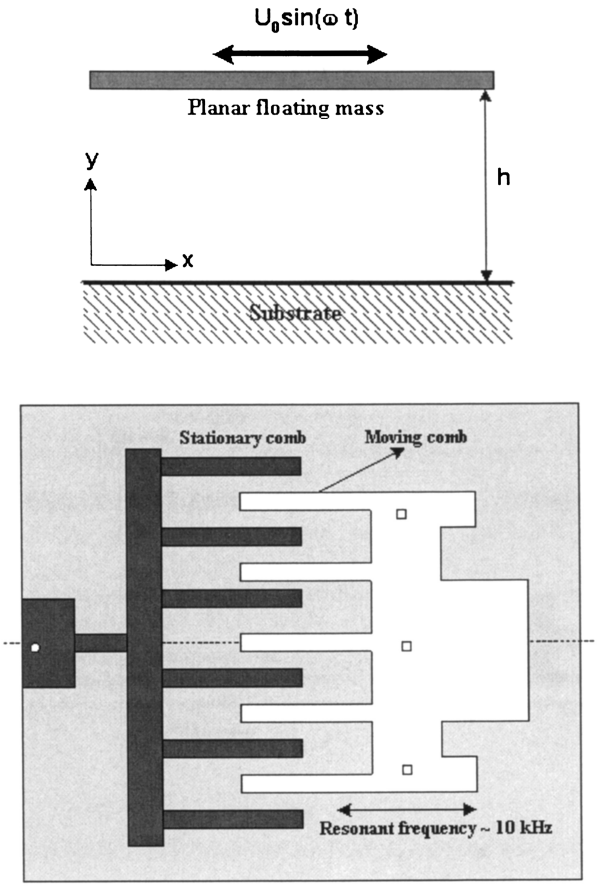

Figure 8. Schematic view of oscillatory Couette flow (top), as an *oversimplified model* of an electrostatic comb drive actuator (bottom).

a balance between the unsteady and viscous effects as

$$\psi = \sqrt{\frac{j\beta^2}{h^2}},$$

where $\beta = \sqrt{\frac{\omega h^2}{\nu}}$ is the Stokes number. Utilizing the slip boundary condition equation (1) with the generalized slip coefficient (α_m), we obtain the following time-dependent velocity distribution: **310**

$$u(y,t) = \Im\left[\left(U_o \frac{\sinh(\sqrt{j}\beta Y) + \sqrt{j}\beta\alpha_m Kn\cosh(\sqrt{j}\beta Y)}{(1+j\beta^2\alpha_m^2 Kn^2)\sinh(\sqrt{j}\beta) + 2\sqrt{j}\beta\alpha_m Kn\cosh(\sqrt{j}\beta)}\right)\exp(j\omega t)\right], \tag{17}$$

where $Y = y/h$ and $Kn = \lambda/h$. This is a *general* solution for the velocity profile that captures the no-slip solution simply by setting $Kn = 0$ and the first-order slip solution

by setting $\alpha_m = 1.111$ in equation (17). Therefore, the above equation is expected to be valid for *any* Stokes number in the continuum and slip flow regimes, as it uniformly captures these well-explored limits; however, the extended model must be validated in the transition and free molecular flow regimes as a function of the Stokes number, which may exhibit richer physics than their continuum and slip regime counterparts. Especially, our new velocity slip model was developed using steady Couette flow results. Hence, its applications to oscillatory flows must be validated, along with the shear stress models.

We performed a series of DSMC simulations for oscillatory Couette flows to assess the validity of the theoretical predictions. The DSMC code used in this study was based on the unsteady algorithm presented by Bird [2]. In all of the following work, we have utilized the Variable Hard Sphere (VHS) collision model [2], and the No-Time-Counter scheme is adapted for collision pair selection. Unlike the HS model, the VHS takes into account the temperature dependence of the transport coefficients, which becomes important for flows with significant temperature variations. We simulated argon gas (molecular mass $m = 6.63 \times 10^{-26} kg$, VHS diameter $d_{vhs} = 4.17 \times 10^{-10} m$) at reference temperature of $T_o = 273K$, with fully accommodating walls. Simulations were performed for a wide range of Knudsen numbers at $\beta = 0.1$ and $\beta = 0.25$ that represent an essentially quasi-steady flow. The spacing between the plates was kept constant at $h = 12.94\mu m$, and the oscillating plate velocity was $U_o = 100m/s$, resulting in $Ma \simeq 0.3$ flow. Therefore, the compressibility and viscous heating effects were negligible. The mean temperature of the medium was found to increase with increasing the oscillation frequency; however, the maximum temperature increase was less than 2%. Gas number density and excitation frequency were adjusted to simulate different combinations of Kn and β, as presented in Table 2.

DSMC simulations of unsteady flows have several cell size and time-step requirements. For example, the simulation time-step Δt must be chosen such that the molecules should not cross more than one cell in between collisions, and Δt must be smaller than the mean collision time, wall oscillation period, and viscous diffusion time-scales. Although the first two conditions are well known in the literature, effects of the boundary-motion period ($\sim 1/\omega$) and viscous diffusion time-scales ($\sim h^2/\nu$) may also become important. In our simulations, the entire domain was discretized into 50 equally spaced cells, and the cell size Δx is chosen smaller than the mean free path for all cases. We have utilized 60 simulated particles per cell, which is significantly larger than the minimum of 20 particles, recommended for accurate DSMC results [21]. Unsteady DSMC computations require ensemble averaging at each time-step. In this study, we simulated the oscillatory

Table 2. Parameters utilized for time-periodic DSMC simulations of oscillatory Couette flows. The separation distance between the two plates is kept constant at $12.94\mu m$

Case	Kn	β	Δt sec	ν m^2/sec	ω rad/sec
1	0.1	0.25	3.838×10^{-9}	3.193×10^{-4}	1.191×10^{5}
2	1	0.25	3.838×10^{-8}	3.193×10^{-3}	1.191×10^{6}
3	2.5	0.25	9.596×10^{-8}	7.982×10^{-3}	2.977×10^{6}
4	2.5	0.1	9.596×10^{-8}	7.982×10^{-3}	4.764×10^{5}
5	5	0.1	1.919×10^{-7}	1.596×10^{-2}	9.529×10^{5}
6	10	0.1	3.838×10^{-7}	3.193×10^{-2}	1.905×10^{6}

flow for three time periods, and ensemble averaged this stochastic process every time-step for over 5,000 realizations.

Overall, our DSMC results show increasing *phase-difference* between the velocity signal imposed on the oscillating wall and the signal felt at the stationary wall for increased Stokes number and rarefaction. Although the phase-difference increase with Stokes number in the continuum flow regime is expected and accurately predicted by solution of equation (13), rarefaction-dependent phase-difference variations have not been reported before. Figure 9 presents time history of the streamwise velocity near the oscillating ($y/h = 0.99$) and stationary ($y/h = 0.01$) walls obtained at various Kn and β conditions. It is important to notice the phase-difference between the DSMC computed velocity signal on the bottom and top walls for the $Kn \leq 10, \beta = 0.1$ case (shown in

Figure 9

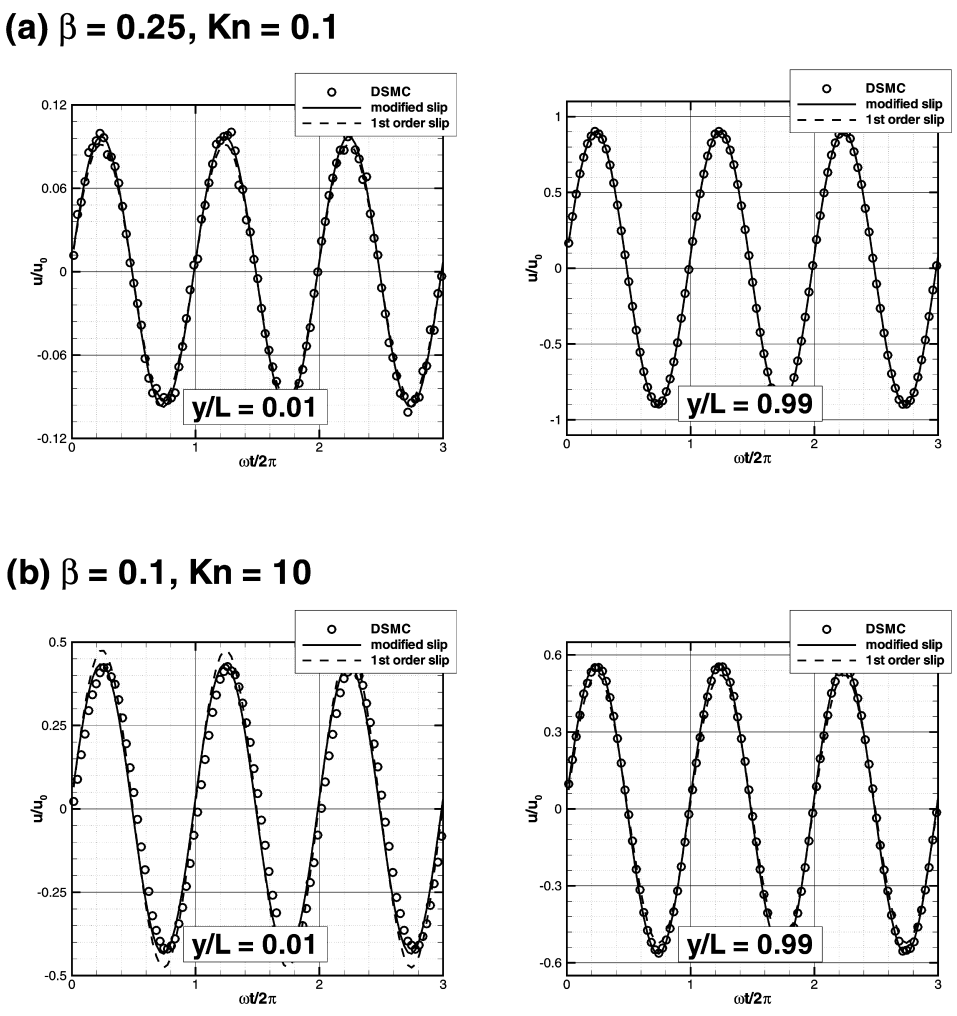

Figure 9. Time variations of the streamwise velocity near the stationary and oscillating walls at (a) $Kn = 0.1$, $\beta = 0.25$ and (b) $Kn = 10$, $\beta = 0.1$ conditions.

figure b). This phase-shift is not as noticeable for the $Kn \leq 0.1$, $\beta = 0.25$ case (shown in figure a).

Figure 9 also shows comparisons between the DSMC results and the new model. The DSMC results accurately capture the slip-flow limit as seen in Figure 9 (a). The generalized velocity model given by equation (17) becomes identical to the first-order slip model for $Kn \leq 0.1$, hence only the predictions of our model is shown in the figure. For $Kn = 10$ and $\beta = 0.1$ simulation, we observe a phase-shift between the DSMC results and the model predictions closer to the stationary wall ($y/h = 0.01$), as shown in Figure 9 (b). The phase shift gradually increases from the oscillating wall to the stationary wall, as seen by comparison of the left and right figures. Figure 10 compares the time history of streamwise velocity for $\beta = 0.1$ and 0.25 flows at $Kn = 2.5$. Hence, this figure

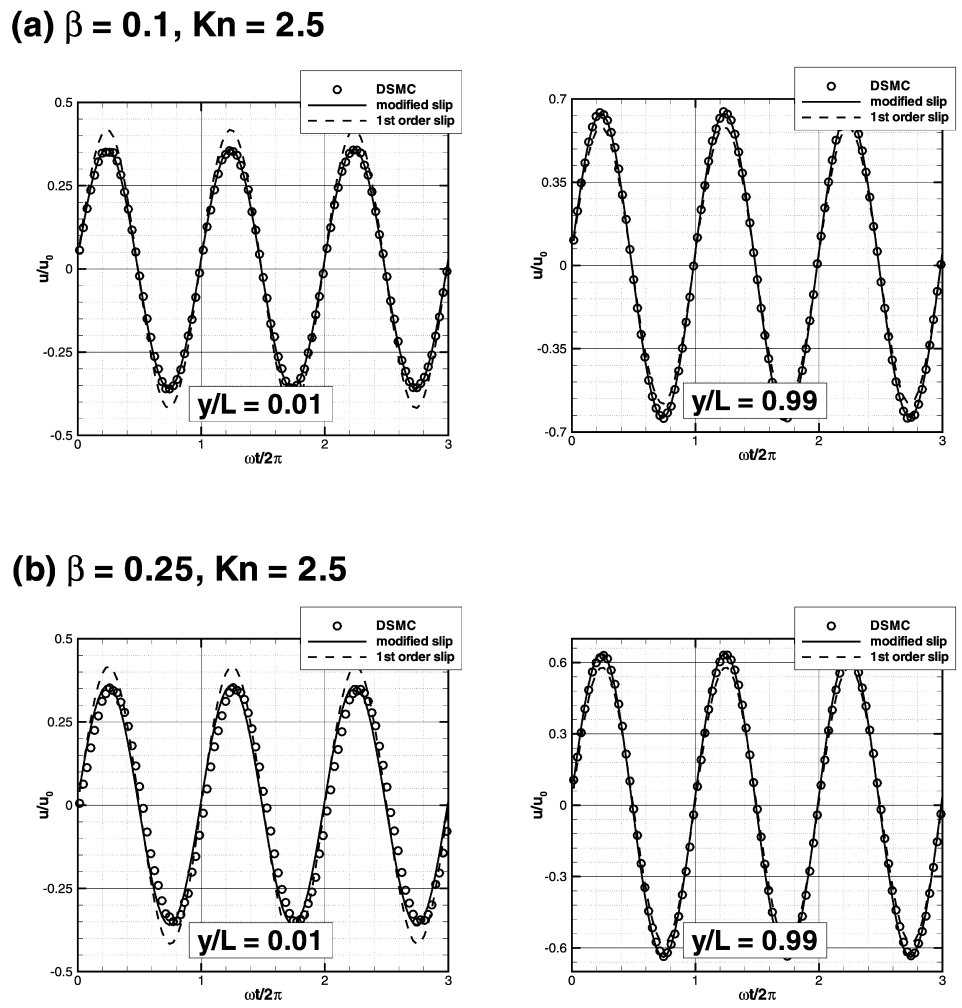

Figure 10. Time variations of the streamwise velocity near the stationary and oscillating walls at (a) $Kn = 2.5$, $\beta = 0.1$ and (b) $Kn = 2.5$, $\beta = 0.25$ conditions.

demonstrates influence of the Stokes number on the phase-difference at fixed Kn. We observe a more pronounced phase-shift between the DSMC results and model predictions closer to the stationary wall ($y/h = 0.01$) for $\beta = 0.25$; however, the phase-difference is almost negligible for the $\beta = 0.1$ case. Our overall observations from Figures 9 and 10 are that the phase-difference between our empirical model and the DSMC results also increases with increased Kn, and β.

Figure 11 shows the normalized velocity amplitudes as a function of the distance from the stationary wall at various Kn and β conditions. Although the first-order slip model gives a reasonable approximation of the velocity amplitude in the slip-flow regime, it systematically deviates from the DSMC results for $Kn > 0.1$. Unlike the first-order model, the generalized model uniformly predicts the velocity amplitudes for a wide range of Knudsen numbers.

We must emphasize that our new model is based on the Navier-Stokes equation with a modified slip condition. Hence, it should practically predict the flow at any Stokes number in the slip and continuum flow regimes. The aforementioned phase-lag between the model and the DSMC results occurs for increased Kn and β values. We believe that discrepancies between the DSMC results and the model are caused by the following two effects: First, there is an inherent phase-shift in the DSMC results with increased Kn, which may be due to the nonequilibrium effects. This physical effect is currently under investigation, and our findings will be reported in subsequent publications. The second effect is model dependent. The modified slip boundary condition is developed using the steady-flow velocity profiles that are *essentially linear in the bulk flow region*. We note that equation (1) with the modified slip coefficient (α_m) is indeed a high-order slip model in Kn (this can be shown via a Taylor series expansion of α_m in Kn); however, the new model lacks high-order derivatives of the velocity profile (such as $\frac{\partial^2 u}{\partial y^2}$), which may become important for high β flows under increased rarefaction ($Kn > 0.1$). Despite these caveats, the new model maintains its accuracy for oscillatory Couette flows for $\beta \leq 0.25$, which is identified as "quasi-steady." Although this may seem to be a significant limitation, our model is applicable for many practical applications. For example, a comb-drive resonator operating with a spacing of $1\mu m$ and oscillation frequency of $\omega = 10kHz$ experiences quasi-steady flow conditions [31]. The Knudsen number will be increased by packaging such flow systems in subatmospheric pressures, which results in increased Kn independent of β. Another alternative is reduction in the gap size, which will increase Kn and further decrease β. Therefore, the quasi-steady flow model developed here is applicable to realistic MEMS applications.

Figure 11

Shear Stress Model

In this section, we extend the shear stress model developed for plane Couette flows to predict the shear stress on the oscillating wall. Using the new velocity model for steady flows and the shear stress model given by equation (10), we define an "effective viscosity" as follows:

$$\mu_{eff} = \frac{(\tau_{xy})_c}{\frac{du_c}{dy}} = \frac{\mu_0}{2}\frac{aKn + 2b}{aKn^2 + cKn + b}(1 + 2\alpha_m Kn), \tag{18}$$

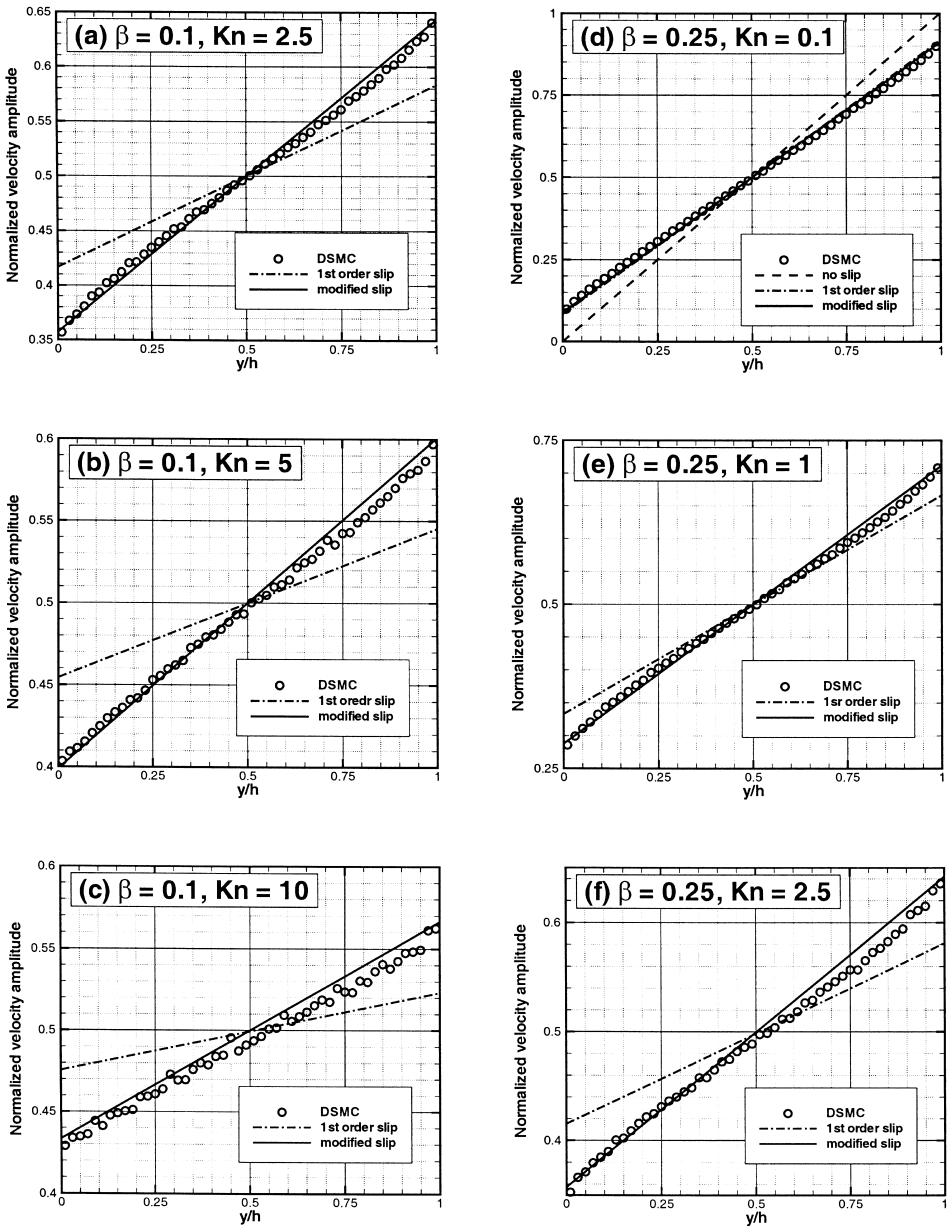

Figure 11. Normalized velocity amplitude as a function of the distance from the stationary wall at various combinations of *Kn* and β. The current model is compared with the *unsteady* DSMC results and the first-order slip model.

where the subscript c indicates plane Couette flow and u_c is the plane Couette flow velocity profile given by equation (3), with the generalized slip coefficient α_m and coefficients a, b, and c due to the shear stress model given in equation (10). For oscillatory flows we use this "effective viscosity" and define the shear stress at the oscillating plate as

$$(\tau_{xy})_{qs} = \mu_{eff} \frac{du(y,t)}{dy}\bigg|_{y=h} = \frac{\mu_0 U_0}{2h} \frac{aKn + 2b}{aKn^2 + cKn + b}(1 + 2\alpha_m Kn)$$

$$\times \Im\left[\left(\sqrt{j}\beta\left(\frac{\cosh(\sqrt{j}\beta) + \sqrt{j}\beta\alpha_m Kn \sinh(\sqrt{j}\beta)}{(1 + j\beta^2\alpha_m^2 Kn^2)\sinh(\sqrt{j}\beta) + 2\sqrt{j}\beta\alpha_m Kn \cosh(\sqrt{j}\beta)}\right)\right)\exp(j\omega t)\right], \tag{19}$$

where subscript qs refers to the quasi-steady flow. Figure 12 shows shear stress time-history at the oscillating wall, normalized with its continuum value, and predictions of the current model and DSMC results are presented for $Kn = 2.5$ flow at $\beta = 0.1$ and 0.25 conditions. There exists a very small magnitude of difference in the shear stress between the $\beta = 0.1$ and 0.25 cases at $Kn = 2.5$. Current model accurately predicts the shear stress magnitude on the oscillating wall, and it also matches the DSMC results for a wide range of Kn values under quasi-steady flow conditions $\beta \leq 0.25$. Figure 13 shows the time-history of the normalized shear stress predicted by the current model for various Kn values and at $\beta = 0.25$ conditions. The new shear stress model developed can be used to compute the damping coefficient in laterally oscillating microstructures.

4. CONCLUSIONS

We have developed empirical models for velocity distribution and shear stress for engineering analysis of shear-driven gas flows encountered in MEMS devices. The new velocity model is based on a generalized slip coefficient, and it uniformly converges to the first-order slip model for $Kn \leq 0.1$ flows while it accurately matches the DSMC and the linearized Boltzmann results in the transition and the free molecular flow regimes. Validity of the velocity model is tested for $Kn \leq 12$. The new shear stress model is valid in the entire Knudsen regime, and it is asymptotically consistent in the continuum ($Kn \to 0$) and free molecular flow ($Kn \to \infty$) regimes. Without detracting from generality or accuracy, these models are valid for monoatomic *dilute hard sphere gases*. Both models are restricted to low subsonic $Ma \leq 0.3$, nearly isothermal flows, as extreme compressibility effects and viscous heating are neglected in their derivation.

The new velocity slip model is also extended to the oscillating Couette flows. It accurately predicts the velocity distribution and the shear stress for quasi-steady flow conditions ($\beta \leq 0.25$). Comparisons between the new model and the unsteady DSMC results have shown a phase-lag for increased β and Kn conditions. Although the new model accurately captures high Stokes number flows in the continuum and slip flow regimes (due to the use of the Navier-Stokes equations in its derivation), onset of the phase-difference between the new model and unsteady DSMC simulations needs to be investigated further.

Our future work on oscillatory Couette flows will concentrate on the DSMC analysis of high Stokes number cases that result in bounded Stokes layers with rarefaction effects. We expect to explore the underlying nonequilibrium physics, especially when

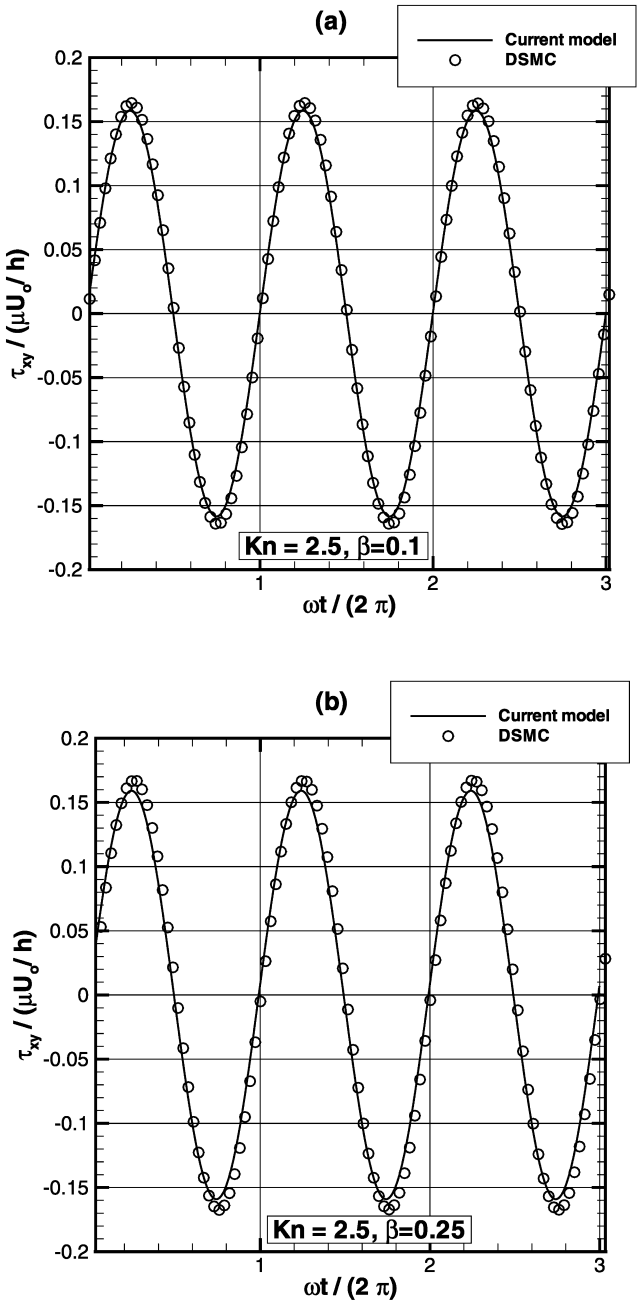

Figure 12. Time history of the normalized shear-stress at the laterally oscillating wall, predicted by the current model and the *unsteady* DSMC simulations at (a) $Kn = 2.5$, $\beta = 0.1$ and (b) $Kn = 2.5$, $\beta = 0.25$.

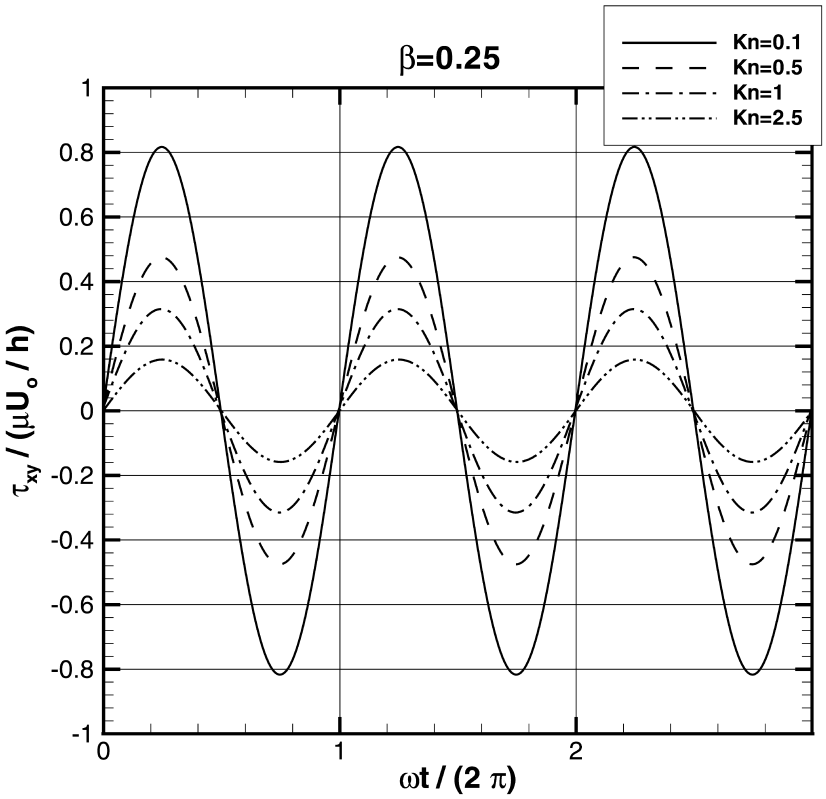

Figure 13. Time history of shear stress at the oscillating wall predicted by the current model for various Knudsen numbers and at Stokes number $\beta = 0.25$.

the oscillation frequency becomes comparable to the mean collision frequency (typically $10^{10} Hz$). In addition, the Stokes layer thickness ($\simeq \sqrt{\nu/\omega}$) creates a new length scale, and one may need to base the characteristic length scale of the problem on the Stokes layer thickness rather than the separation distance between the two plates.

In addition to the steady and oscillatory plane Couette flows, new velocity and shear stress models are also suitable for analysis of rarefied gas flows in slider bearings. This requires integration of the current Couette flow model with the uniformly valid Poiseuille flow model, presented earlier in [13]. We also plan development of gas damping models for laterally oscillating microstructures, such as microresonators and comb-drive actuators.

ACKNOWLEDGMENTS

We would like to thank Dr. Alejandro Garcia for making an early version of his one-dimensional hard-sphere DSMC code available to us. We are grateful to Prof. Felix Sharipov and Prof. Taku Ohwada for many useful discussions and suggestions regarding the current study. JHP acknowledges support by the Post-Doctoral Fellowship Program of Korea Science & Engineering Foundation (KOSEF).

REFERENCES

1. M. Gad-El-Hak, "The fluid mechanics of microdevices," *J. Fluids Engineering*, vol. 12, pp. 5–33, 1999.
2. G. A. Bird, *Molecular Gas Dynamics and the Direct Simulation of Gas Flows*, Oxford Science Publications, Midsomer Norton, Avon, UK, 1994.
3. E. P. Gross and S. Ziering, "Kinetic theory of linear shear flow," *Phys. Fluids A*, vol. 1, pp. 215–224, 1958.
4. D. R. Willis, "Comparison of kinetic theory analyses of linearized Couette flow," *Phys. Fluids A*, vol. 30, pp. 127–135, 1962.
5. S. K. Loyalka, N. Petrellis, and T. S. Storvick, "Some exact numerical results for the BGK model, Couette, Poiseuille and Thermal creep flow between parallel plates," *J. Appl. Math. Phys. (ZAMP)*, vol. 1, pp. 514–521, 1979.
6. C. Cercignani, "A variational principle for boundary value problems in kinetic theory," *J. Stat. Phys.*, vol. 1, pp. 297–311, 1969.
7. J. R. Saraf, "Rarefied gas flows based on variational principle," *J. Stat. Phys.*, vol. 28, pp. 27–36, 1973.
8. Y. Sone, S. Takata and T. Ohwada, "Numerical analysis of the plane Couette flow of a rarefied gas on the basis of the linearized Boltzmann equation for hard sphere molecules," *Eur. J. Mech., B/Fluids*, vol. 9, pp. 273–288, 1990.
9. K. Nanbu, "Analysis of the Couette flow by means of the new direct-simulation method," *J. Phys. Soci. Japan*, vol. 52, pp. 1602–1608, 1983.
10. J. Fan and S. Shen, "Statistical simulation of low-speed rarefied gas flows," *J. Comput. Phys.*, vol. 167, pp. 393–412, 2001.
11. H. Xue, H. M. Ji, and C. Shu, "Analysis of micro-Couette flow using Burnett equations," *Int. J. Heat Mass Transfer*, vol. 44, pp. 4139–4146, 2001.
12. T. Veijola and M. Turowski, "Compact damping models for laterally moving microstructures with gas-rarefaction effects," *J. Microelectromech. Syst.*, vol. 10, pp. 263–273, 2001.
13. G. E. Karniadakis and A. Beskok, *Micro Flows: Fundamentals and Simulation*, Springer-Verlag, New York, 2002.
14. J. C. Maxwell, *Philosophical Transactions of the Royal Society*, London, vol. 170, p. 231, 1867.
15. T. Ohwada, Y. Sone, and K. Aoki, "Numerical analysis of the shear and thermal creep flows of a rarefied gas over a plane wall on the basis of the linearized Boltzmann equation for hard sphere molecules," *Phys. Fluids A*, vol. 1, pp. 1588–1599, 1989.
16. W. Marques, G. M. Kremer, and F. M. Sharipov, "Couette flow with slip and jump boundary conditions," *Continuum Mech. Thermodyn.*, vol. 12, pp. 379–386, 2000.
17. A. L. Garcia, *Numerical Methods for Physics*, Prentice Hall, Upper Saddle River, New Jersey, 2000.
18. E. P. Muntz, "Rarefied gas dynamics," *Ann. Rev. Fluid Mech.*, vol. 21, pp. 387–417, 1989.
19. F. J. Alexander and A. J. Garcia, "The direct simulation Monte Carlo method," *Computers in Phys.*, vol. 11, pp. 588–593, 1997.
20. E. Oran, C. Oh, and B. Cybyk, "Direct Simulation Monte Carlo: Recent advances and applications," *Ann. Rev. Fluid Mech.*, vol. 30, pp. 403–441, 1998.
21. G. Chen and I. D. Boyd, "Statistical error analysis for the direct simulation Monte Carlo technique," *J. Computational Physics*, vol. 126, pp. 434–448, 1996.
22. H. Liepmann and A. Roshko, *Elements of Gas Dynamics*, John Wiley and Sons Inc., New York, 1957.
23. A. Beskok, W. Trimmer, and G. E. Karniadakis, "Rarefaction and Compressibility Effects in Gas Micro-Flows," *J. Fluids Engineering*, vol. 118, pp. 448–456, 1996.

24. R. Schamberg, The Fundamental Differential Equations and the Boundary Conditions for High Speed Slip-Flow, and Their Application to Several Specific Problems, Ph.D. Thesis, California Institute of Technology, California, 1947.
25. D. K. Bhattacharya and G. C. Lie, "Molecular-dynamics simulations of nonequilibrium heat and momentum transport in very dilute gases," *Phys. Rev. Lett.*, vol. 62, pp. 897–900, 1989.
26. D. L. Morris, L. Hannon, and A. L. Garcia, "Slip length in a dilute gas," *Phys. Rev. Lett.*, vol. 46, pp. 5279–5281, 1992.
27. S. Wijesinghe and H. Hadjiconstantinou, "Velocity slip and temperature jump in dilute hard sphere gases at finite Knudsen numbers," *Proc. of the First MIT Conference on Computational Fluid and Solid Mechanics*, vol. 2, pp. 1019–1021, 2001.
28. M. N. Kogan, *Rarefied Gas Dynamics*, Plenum Press, New York, 1969.
29. G. Batchelor, *An Introduction to Fluid Dynamics*, Cambridge University Press, New York, 1998.
30. F. Sherman, *Viscous Flow*, McGraw-Hill, New York, 1990.
31. K. Breuer, Lubrication in MEMS, in M. Gad-El-Hak (ed.), *The MEMS Handbook*, CRC Press, Washington, D.C., 2002.
32. Q. Sun and I. D. Boyd, "A direct simulation method for subsonic, microscale gas flows," *J. Computational Physics*, vol. 179, pp. 400–425, 2002.